photonics

MDPI

Article

Scintillation Properties of β-Ga_2O_3 Under the Excitation of Ultra-High-Charge Electron Bunches

Yulan Liang [1], Jianhan Sun [1], Chaoyi Zhang [2], Tianqi Xu [1], Haoran Chen [1], Huaqing Huang [1], Chenhao Hua [1], Pengying Wan [3,4], Chuanwei Dai [1], Qingfan Wu [1], Juntao Liu [1], Lin Huang [2], Lin Lin [1], Huili Tang [2], Jianming Xue [1], Jun Xu [2], Senlin Huang [1,*], Bo Liu [2] and Wenjun Ma [1,*]

[1] State Key Laboratory of Nuclear Physics and Technology, School of Physics, Peking University, Beijing 100871, China; yulan@stu.pku.edu.cn (Y.L.); sunjianhan@stu.pku.edu.cn (J.S.); 2101110325@stu.pku.edu.cn (T.X.); haoranchen@stu.pku.edu.cn (H.C.); huanghq@stu.pku.edu.cn (H.H.); 2401110324@stu.pku.edu.cn (C.H.); daicw@stu.pku.edu.cn (C.D.); 2201110339@stu.pku.edu.cn (Q.W.); juntaoliu@stu.pku.edu.cn (J.L.); linl@pku.edu.cn (L.L.); jmxue@pku.edu.cn (J.X.)

[2] MOE Key Laboratory of Advanced Micro-Structure Materials, School of Physics Science and Engineering, Tongji University, Shanghai 200092, China; 2011314@tongji.edu.cn (C.Z.); 2311317@tongji.edu.cn (L.H.); tanghl@tongji.edu.cn (H.T.); 15503@tongji.edu.cn (J.X.); lbo@tongji.edu.cn (B.L.)

[3] School of Microelectronics, Xi'an Jiaotong University, Xi'an 710049, China; wanpengying@stu.xjtu.edu.cn

[4] National Key Laboratory of Intense Pulsed Radiation Simulation and Effect, Northwest Institute of Nuclear Technology, Xi'an 710024, China

* Correspondence: huangsl@pku.edu.cn (S.H.); wenjun.ma@pku.edu.cn (W.M.)

Abstract: The performance of ultrafast scintillators under ultrahigh dose rate is highly important for applications utilizing brilliant radiation sources. In this work, the scintillation properties of β-Ga_2O_3, a high-performance ultrafast wide-bandgap semiconductor scintillator, are systematically investigated under dose rates of 10^7 to 10^9 Gy/s for the first time by employing ultrashort high-charge electron bunches (bunch charge from 500 fC to 50 pC) generated from a superconducting radio-frequency accelerator. Our results show that in spite of the ultrahigh dose rate, the scintillation intensity was still linearly proportional to the electron bunch charge. Lifetime analysis reveals a fast decay component ranging from 3 to 4 ns, along with an average lifetime of 20 ns. These findings establish a solid foundation for the application of β-Ga_2O_3 as the scintillation material for high-charge electron sources such as laser-wakefield accelerated electrons.

Keywords: β-Ga_2O_3; high charge; pulsed electron bunch; scintillation properties

Received: 16 December 2024
Revised: 6 February 2025
Accepted: 10 February 2025
Published: 12 February 2025

Citation: Liang, Y.; Sun, J.; Zhang, C.; Xu, T.; Chen, H.; Huang, H.; Hua, C.; Wan, P.; Dai, C.; Wu, Q.; et al. Scintillation Properties of β-Ga_2O_3 Under the Excitation of Ultra-High-Charge Electron Bunches. *Photonics* **2025**, *12*, 149. https://doi.org/10.3390/photonics12020149

1. Introduction

High-energy electrons play a pivotal role in modern light sources and tumor therapy. The cutting-edge technologies of free electron laser (FEL) and FLASH radiotherapy require bunched electrons with ultrashort duration and high charge [1–5]. It is now possible to produce electron bunches with ultrashort duration (fs-ps) and high charge (fC-pC) by utilizing novel acceleration methods such as laser-wakefield acceleration. The precise detection of these electron beams is increasingly vital. Scintillators have been extensively used to measure X-rays and charged particles [6–8]. Its linear responsivity, time response and spectral response are key properties to obtain accurate detection of any radiation field. However, the nonlinearity of scintillation light intensity and lifetime under strong pulse radiations have been observed for many materials excited by high-power laser and strong-pulsed x-ray sources [9–12]. This necessitates calibration of scintillators before practical applications.

Commercially available BaF_2 scintillators demonstrate an ultra-fast decay time of 0.2 ns; however, they exhibit a notably low light yield [13]. In contrast, while Ce-doped inorganic scintillators exhibit higher light yields, their decay times remain insufficiently short for many applications. For example, the decay time of GAGG: Ce scintillator is approximately 90 ns [14], LYSO: Ce has a decay time of around 40 ns [15], and $LaBr_3$: Ce displays a decay time of approximately 20 ns [16]. For β-Ga_2O_3, the light emission resulting from the recombination of self-trapped holes and free electrons has a decay time on the order of a few nanoseconds, accompanied by a theoretical light yield exceeding 40,000 photons per MeV [17]. These characteristics position β-Ga_2O_3 as a promising candidate for inorganic ultrafast scintillators, which could play a significant role in future applications demanding ultra-fast temporal resolution. Moreover, β-Ga_2O_3 is a kind of wide bandgap semiconductor with high radiation resistance and remarkable thermal stability. The melting temperature is measured up to 1793 °C [18]. The structure of β-Ga_2O_3 remain intact even using 400 keV Ar ions of a fluence up to 8×10^{15} cm^2 (equivalent to four displacements per atom) [19]. These advantages render them suitable candidates for strong pulse radiation detections [7,20,21].

Current research on the fluorescence properties of β-Ga_2O_3 primarily utilizes photoluminescence (PL) and x-ray excited luminescence (XEL) [17–22]. Studies on scintillation properties induced by particle excitation remain limited and predominantly employ low dose-rate sources. For instance, Pozina et al. employed scanning electron microscope cathodoluminescence (SEM CL) to explore spectral differences at varying electron excitation densities [23]. He et al. investigated the scintillation response of β-Ga_2O_3 under α-ray excitation from ^{241}Am [24]. Valdes et al. explored the energy dependent scintillation light yield of β-Ga_2O_3 to fast neutrons and gamma rays [25]. However, in applications such as accelerators and FLASH radiotherapy, electron bunches are distinguished by their high energy and high charge. When these electrons interact with the scintillators, they induce energy deposition far exceeding that of the SEM CL and XEL, thereby generating substantial concentration of electron-hole pairs. Under such intense irradiation conditions, the excitation and fluorescence process are likely to change. It is crucial to investigate the scintillation properties of β-Ga_2O_3 under strong-pulsed excitation conditions. However, systematic investigations addressing this aspect remain notably absent from the current literature.

In this study, we aim to investigate the scintillation properties of β-Ga_2O_3 using a pulsed high-charge electron beam generated by a superconducting radio-frequency (SRF) accelerator. Our research reveals the excellent stability of its scintillation characteristics within the electron bunch range of 500 fC to 50 pC for a picosecond-pulsed electron beam, demonstrating the potential of β-Ga_2O_3 for applications utilizing high-charge and ultrashort electron bunches. Furthermore, we also observed that there is a lesser donor–acceptor transition spectral component in high-charge electron excitation compared to SEM CL and XEL. This phenomenon may be associated with the difference in instantaneous carrier density of the excitation, which holds significant implications for future in-depth investigations of luminescence properties at varying dose rates.

2. Materials and Experimental Methods

The unintentionally doped (UID) β-Ga_2O_3 single crystal was grown by the Edge-defined Film-fed Growth method. The growth atmosphere was the mixture of Ar and CO_2 to inhibit decomposition and volatilization of raw material at high temperature. The growth rate was controlled to be 6–15 mm/h. The crystal was obtained by the process of seeding, necking, spreading and equal diameter growth. UID β-Ga_2O_3 crystal sample was (100) plane and double-sided mechanical polishing for the subsequent test.

Absorption spectrum of β-Ga_2O_3 was measured by using a UV–vis–NIR spectrophotometer (UV3600Plus, Shimadzu, Kyoto, Japan). The steady-state photoluminescence and time-resolved photoluminescence spectra were measured using an FLS1000 system (Edinburgh Instruments, Livingston, UK). The XEL was acquired using a Newport spectrometer via a Model 77360 photomultiplier tube with the X-ray tube (12 W X-ray Source, Moxtek Ltd., operating voltage: 30 kV, Orem, UT, USA) served as the excitation source. CL measurements were performed on a field emission scanning electron microscope (Quattro ESEM, Thermo Fisher, Waltham, MA, USA combined with Rainbow-CL of Beijing Goldenscope Technology Co., Ltd., Beijing, China).

In order to investigate the performance of β-Ga_2O_3 under high-charge-pulsed electron excitation, an irradiation platform to measure both in situ time and spectral response was added to the end of a DC-SRF-II photocathode gun beamline at Peking University, as shown in Figure 1a. The energy of electron bunches was measured by a 90° dipole magnet, with a stable energy of 2 MeV. The bunch charge and beam temporal profile were measured using a fast current transformer and a Faraday cup [26,27]. The electron bunches passed through a beryllium window to the air, and the β-Ga_2O_3 was positioned directly outside the vacuum chamber window for irradiation. The scintillation lights were collected using lenses and an optical fiber, then delivered to either the spectrometer (ATP5330/4, Aopu Tiancheng photoelectric Co., Ltd., Xiamen, China) or the photo-multiplier tube (N6012 MCP-PMT of North Night Vision Technology Co., Ltd., Nanjing, China) for spectral analysis and lifetime measurements.

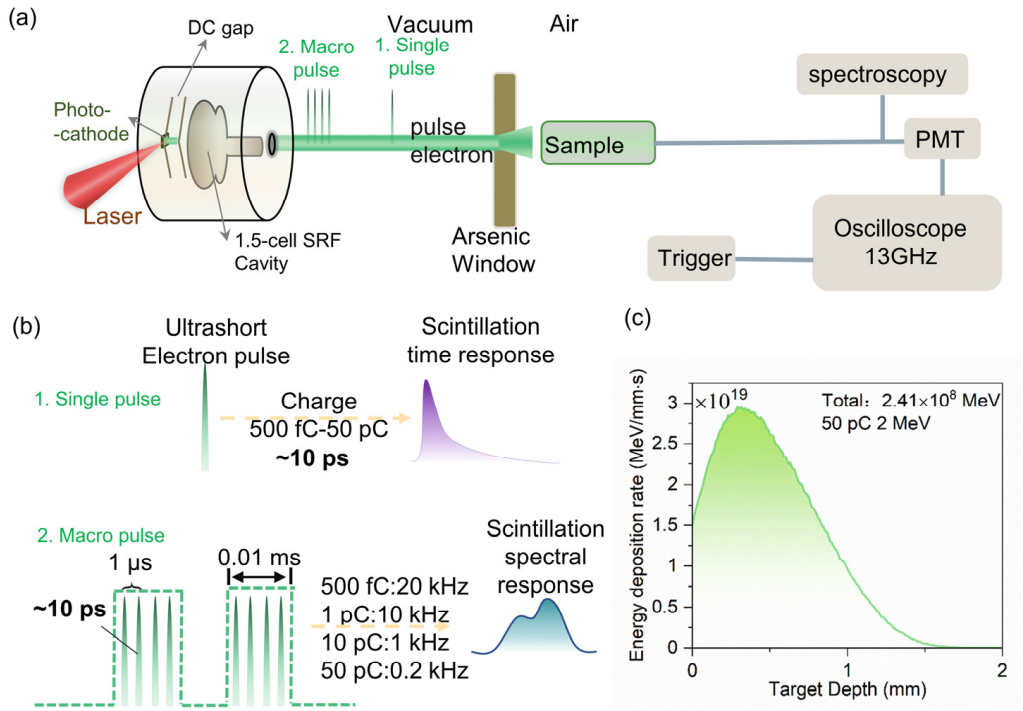

Figure 1. (**a**) The instrumental setup for in situ time and spectral measurements of β-Ga_2O_3 in DC-SRF-II gun beamline at Peking University. (**b**) The temporal profiles of the electron beam for scintillation time/spectral performance characterization of β-Ga_2O_3. (**c**) Simulated total energy deposition rate of 2 MeV pulsed electron beam with 50 pC charge.

The charge of an individual electron bunch and the overall temporal profile of the electron beam can be precisely modulated by adjusting the intensity and temporal profile of the driving laser on the photocathode. In the experiment, we could choose to irradiate the samples using either a single pulse or macro pulses, as depicted in Figure 1b. The single-pulse irradiation was performed at 1 Hz frequency with a narrow width of approximately

10 ps. Macro pulse was formed by multiple short pulses at a period of 1 μs, with a duration of 0.01 ms. The repetition frequency of the macro pulse can be modified from 1 Hz to continuous. The radioluminescence lifetime was measured by employing a single pulse, while the spectra were recorded under macro-pulse excitation. The very narrow 10 ps width of the single pulse allows for accurate measurement of the fast decay component. The repetition of the macro pulses enhances the scintillation intensity and facilitates the detection of spectral signals. By adjusting the repetition frequency to compensate for pulse charge variation, a consistent total irradiated charge can be maintained, effectively reducing the influence of other variables on the experiment.

The initial diameter of the electron bunches was 0.1 mm, which was enlarged after passing through the 250 μm beryllium window. The β-Ga_2O_3 sample had a cross-sectional area of 1 cm × 1 cm and a thickness of 2 mm, positioned 5 mm away from the beryllium. The energy deposition rate was calculated using the Geant4 program, shown in Figure 1c. The simulation setup was designed to replicate the actual experimental conditions. Approximately half of the scattered electrons were captured by the sample according to the simulation. The energy deposition was the integrated energy deposition results on each cross-section, with a longitudinal depth step size of 0.01 mm. For an electron bunch with 50 pC high charge and 2 MeV energy, the total deposited energy reached up to 2.41×10^8 MeV. In the performance study of scintillators, dose and dose rate are typically used for characterization. Dose rate can be calculated from the total deposited energy:

$$DR = \frac{E_n}{\tau \times S \times D \times \rho} \quad (1)$$

τ is the pulse width of the electron bunch, S is the area of the material, D is the range of deposited electron, ρ is the density of the material, and E_n is the total deposited energy. This resulted in a dose rate of 4×10^9 Gy/s, which is several orders of magnitude higher than the dose rates of conventional scintillation characterization methods using x-ray tubes and radioactive sources [28–30]. In our experiments, the dose rate of X-ray source irradiation in XEL was measured to be approximately 400 mGy/s using a dose-rate standard tester. In SEM CL, a current of 3 pA was selected, focused on a scanning area of 50 μm × 50 μm. The average energy of the electrons is 5 keV, with a penetration depth in the micrometer range, resulting in a dose rate of approximately 10^3 Gy/s.

3. Results

3.1. Optical Properties of the Material

The optical absorption spectrum is shown in Figure 2a. The sharp absorption edge is around 250 nm. The inset shows the deduced Tauc plot of $(\alpha hv)^2$ as a function of photon energy, where α is the absorption coefficient and hv is the photon energy. Consequently, it can be observed that the optical bandgap of this β-Ga_2O_3 crystal is 4.71 eV, consistent with previous reported values [31,32]. Figure 2b shows the scintillation decay time excited by 257 nm pulsed laser using FLS1000. Fitted by the bi-exponential decay curve, the fast/slow component is 11.67 ns (38.9%)/58.72 ns (61.1%). The averaged decay time is 40.41 ns, consistent with previous studies [33–35]. Figure 2c shows the photoluminescence (PL) spectra. A broad spectrum from 2.5 eV to 4 eV is presented under the excitation of 240 nm. It can be decomposed into two Gaussian luminescence bands, 3.4 eV (68.66%) and 3.1 eV (31.34%). The luminescence processes are schematically illustrated in Figure 2d. The 3.4 eV (UV band) peak luminescence is independent of sample preparation methods or dopants [7]. It is attributed to an intrinsic luminescent process arising from the recombination of self-trapped holes and free electrons, with emission energies ranging from 3.2 to 3.7 eV. The 3.1 eV (UV' band) peak is the result of the donor–acceptor luminescence [23,36].

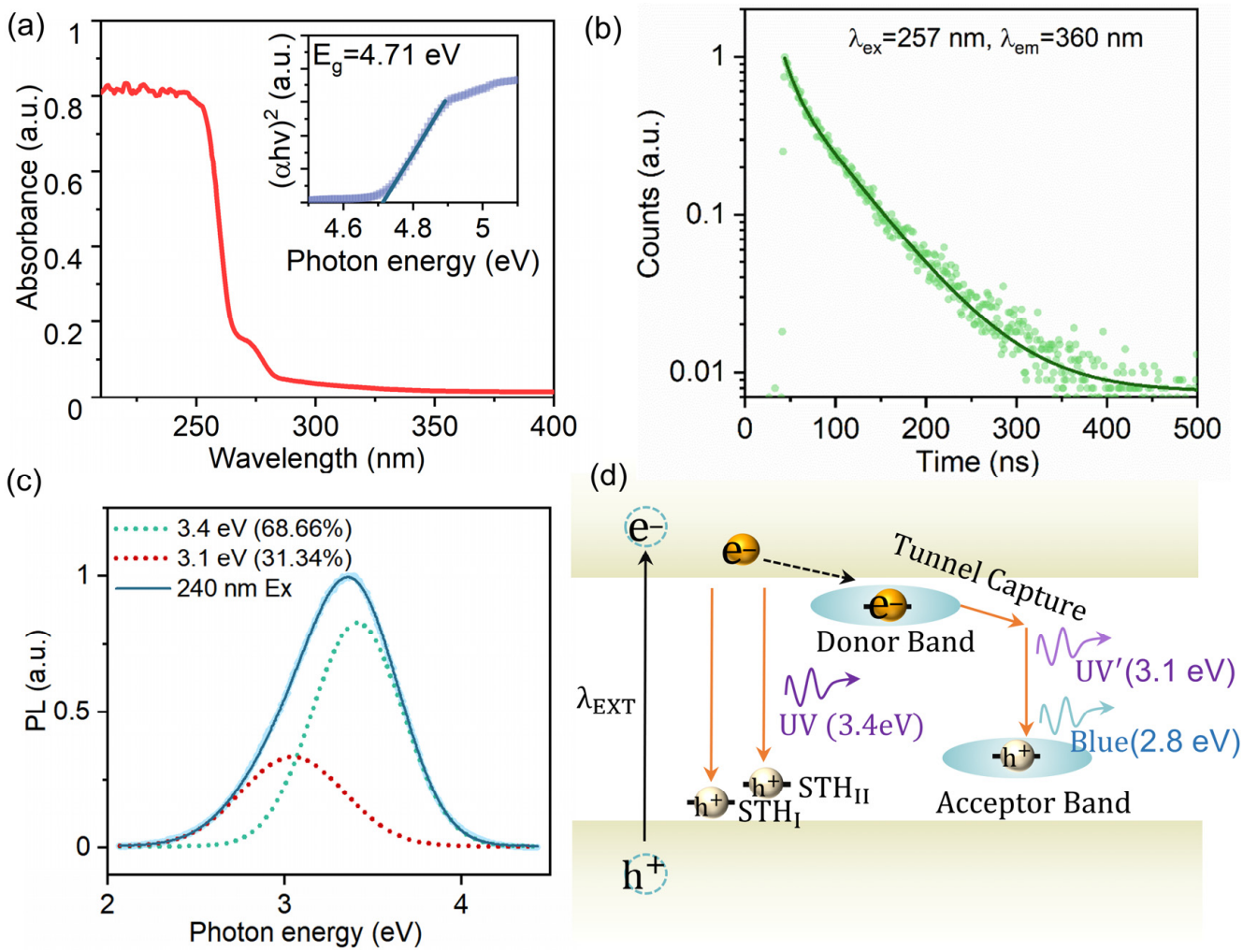

Figure 2. (**a**) Optical absorption spectra of β-Ga_2O_3. The inset shows the Tauc plot of the bulk crystal. (**b**) Scintillation time response of β-Ga_2O_3 excited by 257 nm pulsed laser. (**c**) The PL spectra measured by 240 nm Xe lamp. The dashed lines represent the Gaussian fitting results, with the red line corresponding to 3.1 eV and the green line corresponding to 3.4 eV. (**d**) Illustration of the emission paths leading to the observed peaks for PL.

3.2. Time Response of Scintillation Excited by High-Charge Electron Bunches

The spectra measured by the spectrometer were integrated to obtain the corresponding scintillation intensity. The integrated scintillation light intensity reveals a strong linear correlation with the electron charge, as depicted in Figure 3a. This demonstrates the remarkable linearity of β-Ga_2O_3 under high-charge electron bunch excitation, thereby confirming its suitability as a scintillator for relevant applications.

The time response of the scintillation detector is of vital importance. We measured the scintillation decay time of β-Ga_2O_3 for different electron bunch charges with the single-bunch pulse width of 10 ps. The raw data are shown in Figure 3b. With a decrease in beam charge, the luminescence intensity of the material diminishes. Nevertheless, the scintillation time curve characteristics remain essentially unaltered. All the decay time are fitted by a sum of two exponential decay functions, with the decay time constant and relative portion summarized in Table 1. The average decay time was calculated from the equation:

$$\tau_{ave} = \frac{\tau_1 A_1 + \tau_2 A_2}{A_1 + A_2} \quad (2)$$

where A_1, A_2 are the amplitudes and τ_1, τ_2 denote the time constants.

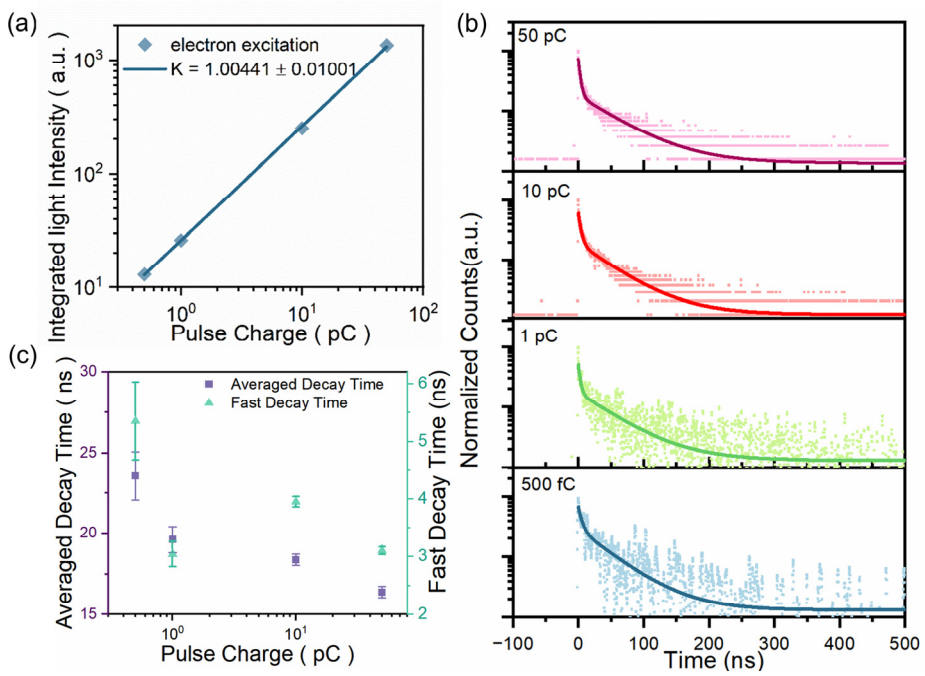

Figure 3. (**a**) A plot of log (integrated light intensity) vs. log (pulse charge). Solid lines are the linear fitting curves. (**b**) Time-resolved decay curves under pulsed electron bunch excitation of different charge levels. (**c**) The averaged decay time and the fast decay time components for different dose rates derived from different charges in the 10 ps electron bunch.

Table 1. The decay constant of β-Ga_2O_3 under high-charge electron bunch excitation.

Bunch Charge (pC)	Dose Rate (Gy/s)	τ_1 (ns)	τ_2 (ns)	Averaged Decay Time τ (ns)
0.5	4×10^7	5.35 (60.22%)	51.14 (39.78%)	23.57
1	8×10^7	3.04 (69.20%)	56.83 (30.80%)	19.61
10	8×10^8	3.95 (71.16%)	53.92 (28.84%)	18.36
50	4×10^9	3.10 (76.45%)	59.49 (23.55%)	16.38

The averaged decay time and the fast decay time component are plotted in Figure 3c. The average decay time was found to be approximately 20 ns, which is significantly faster than the commercially available Ce-doped inorganic scintillators [14,15]. As the electron charge increases, the transient concentration of excited carriers rises, and the average decay time exhibits a trend of decreasing duration. This may be attributed to the fact that under high-density excitation, the excess carriers greatly exceed the intrinsic carriers, leading to the manifestation of bimolecular processes [37]. The average decay time is faster than that of PL. Moreover, the fast-emitting fraction exhibits a notably shorter decay time of approximately 3–4 ns, which is three times briefer than the 11 ns PL lifetime. Figure 3c also shows the results of the fast decay component under different pulse charges. Overall, the fast decay lifetimes are less than 6 ns. As shown in Table 1, the fast component dominates, contributing over 60% of the total signal. Notably, as the pulse charge increases, both the fast decay speed and the proportion of the fast component rise, highlighting the significant potential of this material for next-generation ultrafast scintillation detection systems.

3.3. Scintillation Spectral

Figure 4a shows the luminescence spectrum of β-Ga_2O_3 under high-charge electron bunch (HCEB) excitation. It exhibits a lower signal-to-noise ratio compared to other methods, which can be attributed to the reduced signal transmission efficiency inherent in the long-distance optical fiber coupling. Despite the relatively low signal-to-noise ratio, Figure 4a still clearly reveals the luminescent band of β-Ga_2O_3 in the range of 2.5 to 4 eV. The acquired spectra were analyzed using Gaussian fitting. The predominant luminescence component is the UV band emission at 3.4 eV. However, it changes from 68.7% to 51.7% compared with PL in Figure 2c. Moreover, compared with PL, an additional blue band emission peak at 2.8 eV was presented. As mentioned, the UV band emission is regarded as intrinsic. In contrast, other luminescent bands, the UV′ (3.1 eV) and the blue band (2.8 eV) are a donor–acceptor pair (DAP) luminescence and are associated with various defects or impurities. The difference arises primarily from variations in defect types [36]. Typical donor defects include V_O and Ga_i, while acceptor defects are generally V_O-V_{Ga} or V_{Ga} [38]. The appearance of the 2.8 eV suggests that deeper defects are involved in the radiative recombination process of electron-excited scintillation. The discrepancy from the PL spectra may be attributed to the different defect concentrations induced by surface excitation in PL and bulk excitation in electron bunch-induced luminescence.

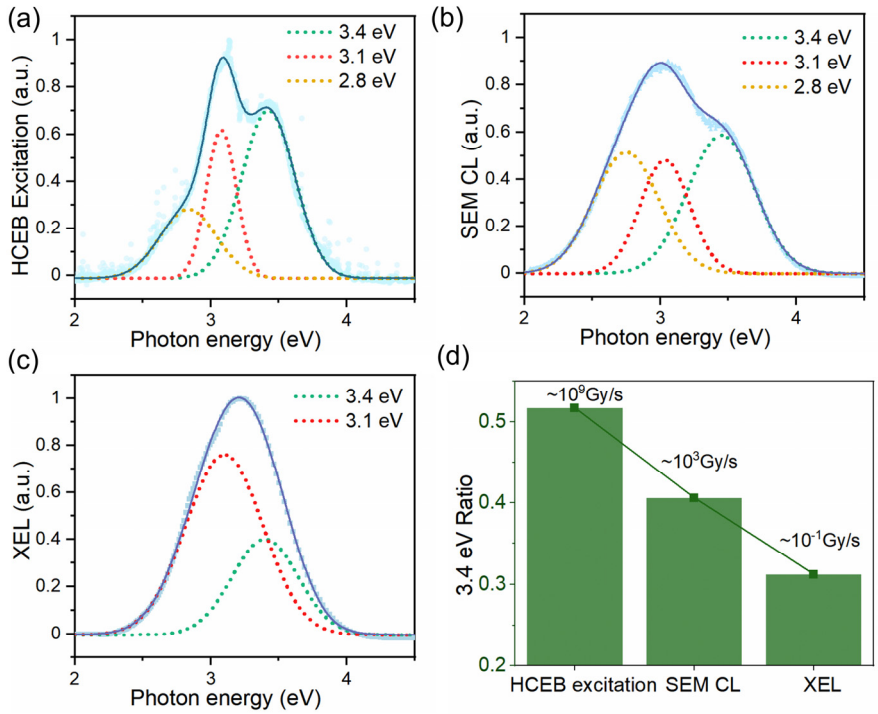

Figure 4. (**a**) Normalized spectral response of β-Ga_2O_3 under HCEB excitation of 50 pC with its Gaussian fitting results. (**b**) Normalized SEM CL spectra of β-Ga_2O_3. (**c**) Normalized XEL spectrum of β-Ga_2O_3. (**d**) The ratio of the area difference of 3.4 eV peak for different excitation methods.

To investigate the differences in the scintillation characteristics of β-Ga_2O_3 under various conditions, we also measured the luminescence spectra under the excitation of SEM CL and XEL for the same set of samples. The SEM CL result is shown in Figure 4b. It can be decomposed into three components. The proportion of the 3.4 eV component decreases. Emissions at 2.8 eV and 3.1 eV are attributed to defect-related luminescence and can be collectively categorized as DAP luminescence. At this point, the contribution from DAP luminescence increases, indicating that more defects are involved in the luminescence process. In the case of XEL (Figure 4c), even when fitting with three Gaussian curves, the

data can only be well represented by decomposing it into the 3.4 eV and 3.1 eV components. This suggests that in XEL, the defect-related luminescence is primarily concentrated around 3.1 eV, corresponding to shallower energy level defects.

Figure 4d shows the area ratio difference of UV band emission (peak 3.4 eV) for different irradiation sources. Under HCEB excitation, the UV band emission exhibits a significant enhancement, with the contribution to the total luminescence almost doubling in comparison to that of XEL. This indicates that UV band emission predominates in this condition. We present a detailed comparison of the different spectral components relative to the total luminescence intensity under various conditions, as summarized in Table 2. Notably, the 3.1 eV emission constitutes the predominant portion of the XEL luminescence, with no contribution from the 2.8 eV component. In contrast, both the 3.1 eV and 2.8 eV emissions are observed in SEM CL and HCEB excitation luminescence. This discrepancy may be attributed to the differing excitation mechanisms involved in X-ray versus electron excitation. Under HCEB excitation, the proportion of 3.1 eV emission is higher, while in SEM CL, the contributions from both types of defects are comparable. This difference may be attributed to the variations in excitation depth and luminescent properties caused by electrons of different energies.

Table 2. The variation of peaks of β-Ga_2O_3 as a function of excitation methods.

Excitation Methods	3.4 eV	DAP	3.1 eV	2.8 eV
XEL	31.2%	68.8%	68.8%	0
SEM CL	40.6%	59.4%	24.5%	34.9%
HCEB excitation	51.7%	48.3%	25.7%	22.6%

In order to explore whether the luminescence spectra of β-Ga_2O_3 are stable under the excitation of high-charge electron irradiation, experiments were conducted by varying the electron charges in a macro pulse, as shown in Figure 5a. Remarkably, the shape of the spectrum exhibits negligible changes across 500 fC to 50 pC (approximately 10^7 Gy/s to 10^9 Gy/s for a single bunch), suggesting that the emission bands remain relatively unaltered. The relative contributions of each emission peak were quantified and presented in Figure 5b, where different groups correspond to specific excitation conditions. This indicates that the radiation damage has a negligible impact on the spectral results across varying excitation dose rates (different electron bunch charges), which further demonstrate the stability of β-Ga_2O_3 under high charge (500 fC to 50 pC) and high dose rate (10^7 Gy/s to 10^9 Gy/s) electron irradiation.

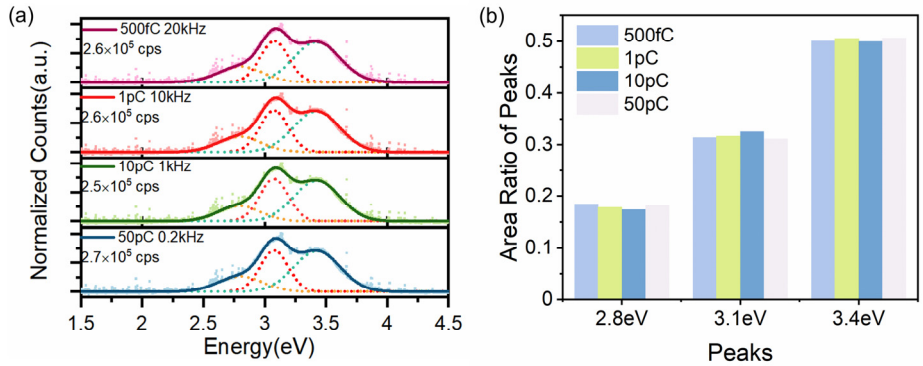

Figure 5. (**a**) Luminescence spectra of β-Ga_2O_3 under HCEB excitation of different charge levels. The dashed lines represent the Gaussian fitting results, with the orange line corresponding to 2.8 eV, the red line corresponding to 3.1 eV and the green line corresponding to 3.4 eV. (**b**). Area ratio of different peaks (3.4 eV, 3.1 eV, 2.8 eV).

4. Discussion

The spectra of XEL, SEM CL, and HCEB excitation luminescence exhibit significant differences. The interaction of keV X-rays with matter predominantly generates secondary electrons via the photoelectric effect, thereby exhibiting a certain level of theoretical equivalence. Comparatively, XEL exhibited the lowest dose rate (400 mGy/s). In SEM CL, a current of 3 pA was used over a 50 μm × 50 μm scanning area, with an average electron energy of 5 keV. This setup yields a penetration depth in the micrometer range and a dose rate of approximately 10^3 Gy/s. HCEB excitation luminescence demonstrated the highest dose rate (up to 10^9 Gy/s). Through a comparison of spectral data, it was observed that with increasing dose rates, the proportion of UV-band emission rises, while the DAP luminescence correspondingly diminishes. Under lower excitation densities, the preferential relaxation of electrons and holes are to band edges and subsequently captured by inter-band defects. As a result, the predominant recombination path is via DAP. However, at considerably high dose rates, defects may become saturated, enabling a greater contribution from UV band emission. Similar trends were reported by Pozina et al. in 2017 when varying the current of the SEM [23]. A closer examination of the 3.1 eV and 2.8 eV components indicates that under the XEL excitation, only the 3.1 eV luminescence is observed. In contrast, both SEM CL and HCEB excitation luminescence exhibit comparable contributions from the 3.1 eV and 2.8 eV emissions. This discrepancy may be attributed to the difference in secondary electron generation and thermal relaxation associated with X-ray and electron excitation methods. Li et al. emphasized the impact of various excitation sources on the luminescence of $Cs_3Cu_2I_5$, noting that X-ray excitation tends to capture more electrons directly into the inter-band energy levels compared to UV photon excitation, leading to emission in different spectral ranges [39]. Furthermore, the varying penetration depths of electrons with different energies may invoke different defect species within the material. These findings underscore the importance of categorizing irradiation types, energy levels, and dose rates in the field of scintillation physics. Nevertheless, the spectral changes within our dose rate parameter window (10^7 Gy/s to 10^9 Gy/s) are relatively minor, which is consistent with the results in Figure 3 where a clear linear response is observed.

As for the case of time response for high-charge electron excitation, the fast decay component is almost three times as fast as that for PL emissions. However, the average decay time is only twice as fast. The initial rapid decay time was likely attributed to the quenching effects induced by higher-order processes. Diverging from the through-band excitation in PL, high-energy electrons can generate secondary electrons through inelastic scattering. They then facilitate localized carrier accumulation and promote exciton–exciton annihilation and Auger recombination processes, which exhibit a polynomial relationship with carrier concentration and can expedite the fluorescence decay rate [40,41]. However, it is noteworthy that the measured lifetimes of donor–acceptor emissions exhibit slower time constants compared to the UV-band emission [42]. Spectral analysis reveals that under HCEB excitation, the contribution of the UV-band emission diminishes compared to PL. The increased number of deeper defect levels participating in the radiative recombination process can lead to a substantial augmentation in the proportion of long-lived components. Therefore, the slow decay component of HCEB excitation of different pulse charges is comparable or even a bit longer than that of PL. Taking these two factors into account, the averaged decay time for HCEB excitation is approximately twice as fast as that for PL emissions. As for the decay time under the electron accelerator excitation, the fast decay times are consistently under 6 ns, with the fast component dominating the total signal at over 60%. As the dose rate increases, the average lifetime remains around 20 ns, which is significantly faster than the commercially available inorganic scintillators like GAGG: Ce [14]. This highlights the material's considerable potential for future ultrafast scintillation detection

systems. Moreover, both the average decay time and the fast decay time components exhibit a decreasing trend. This may involve some bimolecular processes under high-density excitation [37], which will be systematically investigated in future experiments.

These results underscore the distinct differences in luminescence physics and properties compared to conventional low-energy, low-dose-rate electron, X-ray excitation and laser excitation. Consequently, it is imperative to perform performance tests on scintillators under relevant high-charge ultrashort conditions for practical strong-pulsed radiation detection applications. The precise condition at which significant changes occur in the properties of β-Ga_2O_3 and the specific inflection point are still ambiguous, necessitating further comprehensive research and analysis. Nevertheless, our results demonstrate the intrinsic stability of β-Ga_2O_3 in emission characteristics, including emission spectrum, linear responsivity and fast-decay time, across pulse charges ranging from 500 fC to 50 pC with pulse width of 10 ps.

5. Conclusions

In conclusion, this study presents the first investigation into the time and spectral characteristics of β-Ga_2O_3 under the excitation of electrons with ultra-high charge and ultrashort pulse duration. Remarkably, the luminescence intensity of β-Ga_2O_3 exhibits a strong linear correlation with the charge of incident electrons in the range of 500 fC to 50 pC (dose rate within the range of 10^7 to 10^9 Gy/s). Lifetime analysis reveals a fast decay component ranging from 3 to 4 ns, along with an average lifetime of 20 ns. The obtained spectrum exhibits prominent peaks at 2.8 eV, 3.1 eV, and 3.4 eV, remaining stable across 500 fC to 50 pC charge levels. These findings provide a solid basis for the application of β-Ga_2O_3 as a scintillation detector in high-charge electron bunches. Our comparative analysis of the emission spectra with XEL and SEM CL reveals that with increasing dose rates, the proportion of UV-band emission rises, while the DAP luminescence correspondingly diminishes. This underscores the importance of categorizing irradiation types, energy levels, and dose rates in the field of scintillation physics. Consequently, it is imperative to conduct performance tests on scintillators under relevant strong-pulsed radiation conditions for practical detection applications. In future studies, comprehensive experiments and analysis are necessary to elucidate the underlying mechanisms.

Author Contributions: Conceptualization, Y.L. and W.M.; methodology, Y.L., J.S., Q.W., L.L., S.H., B.L. and W.M.; software, J.S., C.D. and Y.L.; validation, Y.L., J.S. and J.L.; formal analysis, Y.L.; investigation, Y.L., J.S., T.X., H.C., H.H., C.H., P.W., J.L. and L.L.; resources, C.Z., L.H., J.X. (Jun Xu) and H.T.; data curation, Y.L.; writing—original draft preparation, Y.L.; writing—review and editing, Y.L., S.H., B.L. and W.M.; visualization, Y.L.; supervision, B.L. and W.M.; project administration, S.H., J.X. (Jianming Xue), B.L. and W.M.; funding acquisition, S.H., H.T., B.L. and W.M. All authors have read and agreed to the published version of the manuscript.

Funding: This work was supported by the following projects: the National Grand Instrument Project (Grant No. 2019YFF01014402), the National Natural Science Foundation of China (No. 12375181) and the National Key Research and Development Program of China (Grant No. 2017YFA0701001). W. Ma acknowledges support from the National Science Fund for Distinguished Young Scholars (No. 12225501).

Institutional Review Board Statement: Not applicable.

Informed Consent Statement: Not applicable.

Data Availability Statement: The data presented in this study will be made available by the authors on request.

Conflicts of Interest: The authors declare no conflicts of interest.

References

1. Mangles, S.P.; Murphy, C.D.; Najmudin, Z.; Thomas, A.G.; Collier, J.L.; Dangor, A.E.; Divall, E.J.; Foster, P.S.; Gallacher, J.G.; Hooker, C.J.; et al. Monoenergetic beams of relativistic electrons from intense laser-plasma interactions. *Nature* **2004**, *431*, 535–538. [CrossRef] [PubMed]
2. Geddes, C.G.; Toth, C.S.; Van Tilborg, J.; Esarey, E.; Schroeder, C.B.; Bruhwiler, D.; Nieter, C.; Cary, J.; Leemans, W.P. High-quality electron beams from a laser wakefield accelerator using plasma-channel guiding. *Nature* **2004**, *431*, 538–541. [CrossRef] [PubMed]
3. Feist, A.; Bach, N.; Rubiano da Silva, N.; Danz, T.; Moller, M.; Priebe, K.E.; Domrose, T.; Gatzmann, J.G.; Rost, S.; Schauss, J.; et al. Ultrafast transmission electron microscopy using a laser-driven field emitter: Femtosecond resolution with a high coherence electron beam. *Ultramicroscopy* **2017**, *176*, 63–73. [CrossRef] [PubMed]
4. Vozenin, M.C.; Bourhis, J.; Durante, M. Towards clinical translation of FLASH radiotherapy. *Nat. Rev. Clin. Oncol.* **2022**, *19*, 791–803. [CrossRef]
5. McManus, M.; Romano, F.; Lee, N.D.; Farabolini, W.; Gilardi, A.; Royle, G.; Palmans, H.; Subiel, A. The challenge of ionisation chamber dosimetry in ultra-short pulsed high dose-rate Very High Energy Electron beams. *Sci. Rep.* **2020**, *10*, 9089. [CrossRef]
6. Gardés, E.; Balanzat, E.; Ban-d'Etat, B.; Cassimi, A.; Durantel, F.; Grygiel, C.; Madi, T.; Monnet, I.; Ramillon, J.M.; Ropars, F.; et al. SPORT: A new sub-nanosecond time-resolved instrument to study swift heavy ion-beam induced luminescence—Application to luminescence degradation of a fast plastic scintillator. *Nucl. Instrum. Methods Phys. Res. Sect. B Beam Interact. Mater. At.* **2013**, *297*, 39–43. [CrossRef]
7. He, N.; Tang, H.; Liu, B.; Zhu, Z.; Li, Q.; Guo, C.; Gu, M.; Xu, J.; Liu, J.; Xu, M.; et al. Ultra-fast scintillation properties of β-Ga_2O_3 single crystals grown by Floating Zone method. *Nucl. Instrum. Methods Phys. Res. Sect. A Accel. Spectrometers, Detect. Assoc. Equip.* **2018**, *888*, 9–12. [CrossRef]
8. Koshimizu, M.; Kimura, A.; Kurashima, S.; Taguchi, M.; Yanagida, T.; Fujimoto, Y.; Asai, K. Effect of linear energy transfer on the scintillation properties of Ce-doped $Ca_3B_2O_6$ crystals. *Nucl. Instrum. Methods Phys. Res. Sect. B-Beam Interact. Mater. At.* **2020**, *471*, 59–62. [CrossRef]
9. Chen, X.; Han, H.-T.; Li, G. Experimental study on high dose rate response of cadmium zinc telluride detectors to pulsed X-ray. *Radiat. Meas.* **2017**, *97*, 42–46. [CrossRef]
10. Grim, J.Q.; Ucer, K.B.; Burger, A.; Bhattacharya, P.; Tupitsyn, E.; Rowe, E.; Buliga, V.M.; Trefilova, L.; Gektin, A.; Bizarri, G.A.; et al. Nonlinear quenching of densely excited states in wide-gap solids. *Phys. Rev. B* **2013**, *87*, 125117. [CrossRef]
11. Laasner, R.; Fedorov, N.; Grigonis, R.; Guizard, S.; Kirm, M.; Makhov, V.; Markov, S.; Nagirnyi, V.; Sirutkaitis, V.; Vasil'ev, A.; et al. Band tail absorption saturation in $CdWO_4$ with 100 fs laser pulses. *J. Phys. Condens. Matter* **2013**, *25*, 245901. [CrossRef] [PubMed]
12. Guan, X.; Zhang, Z.; Zhang, W. Measurement of Linear Response Upper Limit for Lutecium Oxyorthosilicate Scitillator in High Dose Rate to Pulsed Gamma Radiation. *At. Energy Sci. Technol.* **2009**, *43*, 942–945.
13. Peng, C.; Zhang, K.; Yang, L.; Zheng, J.Q.; Lu, Y.; Hou, Y.Y.; Yan, X.L.; Shi, Z.J.; Han, H.T.; Song, Z.H.; et al. Investigation on the Fast Component Light Yield of BaF2: Y Crystal. *IEEE Trans. Nucl. Sci.* **2022**, *69*, 2083–2088. [CrossRef]
14. Yanagida, T.; Kamada, K.; Fujimoto, Y.; Yagi, H.; Yanagitani, T. Comparative study of ceramic and single crystal Ce: GAGG scintillator. *Opt. Mater.* **2013**, *35*, 2480–2485. [CrossRef]
15. Xue, Z.; Chen, L.; Zhao, S.; Yang, F.; An, R.; Wang, L.; Sun, Y.-Y.; Feng, H.; Ding, D. Enhancement of scintillation properties of LYSO: Ce crystals by Al codoping. *Cryst. Growth Des.* **2023**, *23*, 4562–4570. [CrossRef]
16. Pustovarov, V.A.; Razumov, A.N.; Vyprintsev, D.I. Luminescence of LaBr3: Ce, Hf crystals under photon excitation in the ultraviolet, vacuum ultraviolet, and X-ray ranges. *Phys. Solid State* **2014**, *56*, 347–352. [CrossRef]
17. Mykhaylyk, V.B.; Kraus, H.; Kapustianyk, V.; Rudko, M. Low temperature scintillation properties of Ga_2O_3. *Appl. Phys. Lett.* **2019**, *115*, 081103. [CrossRef]
18. Hoshikawa, K.; Ohba, E.; Kobayashi, T.; Yanagisawa, J.; Miyagawa, C.; Nakamura, Y. Growth of β-Ga_2O_3 single crystals using vertical Bridgman method in ambient air. *J. Cryst. Growth* **2016**, *447*, 36–41. [CrossRef]
19. Petkov, A.; Cherns, D.; Chen, W.-Y.; Liu, J.; Blevins, J.; Gambin, V.; Li, M.; Liu, D.; Kuball, M. Structural stability of β-Ga_2O_3 under ion irradiation. *Appl. Phys. Lett.* **2022**, *121*, 171903. [CrossRef]
20. Tang, H.; He, N.; Zhu, Z.; Gu, M.; Liu, B.; Xu, J.; Xu, M.; Chen, L.; Liu, J.; Ouyang, X. Temperature-dependence of X-ray excited luminescence of β-Ga_2O_3 single crystals. *Appl. Phys. Lett.* **2019**, *115*, 071904. [CrossRef]
21. Li, Z.; Tang, H.; Li, Y.; Gu, M.; Xu, J.; Chen, L.; Liu, J.; Ouyang, X.; Liu, B. Enhanced scintillation performance of β-Ga_2O_3 single crystals by Al3+ doping and its physical mechanism. *Appl. Phys. Lett.* **2022**, *121*, 102102. [CrossRef]
22. Stepanov, S.I.; Nikolaev, V.I.; Bougrov, V.E.; Romanov, A.E. Gallium Oxide: Properties and Applications—A Review. *Rev. Adv. Mater. Sci.* **2016**, *44*, 63–86.
23. Pozina, G.; Forsberg, M.; Kaliteevski, M.A.; Hemmingsson, C. Emission properties of Ga_2O_3 nano-flakes: Effect of excitation density. *Sci. Rep.* **2017**, *7*, 42132. [CrossRef]
24. He, N.; Ouyang, X.; Xu, M.; Tang, H.; Liu, B.; Zhu, Z.; Gu, M.; Xu, J.; Liu, J.; Chen, L. Scintillation Properties of β-Ga_2O_3 Single Crystal Excited by α-Ray. *IEEE Trans. Nucl. Sci.* **2020**, *67*, 400–404. [CrossRef]

25. Valdes, D.J.; Miller, S.; Leak, C.; Haque, S.; Gunthoti, K.; Wender, S.A.; Paneru, S.; Lee, H.Y.; Vogel, S.C.; Sun, K.X. Gallium oxide (Ga2O3) energy dependent scintillation response to fast neutrons and flash gamma-rays. *Rev. Sci. Instrum.* **2024**, *95*, 083549. [CrossRef]
26. Jia, H.; Li, T.; Wang, T.; Zhao, Y.; Zhang, X.; Xu, H.; Liu, Z.; Liu, J.; Lin, L.; Xie, H.; et al. High-brightness megahertz-rate beam from a direct-current and superconducting radio-frequency combined photocathode gun. *Phys. Rev. Res.* **2024**, *6*, 043165. [CrossRef]
27. Sun, J.; Lv, J.; Tian, S.; Liu, J.; Zhang, Z.; Xu, H.; Lin, L.; Huang, S. Dosimetry study of high repetition rate MeV electron beam from a continuous-wave photocathode gun. *arXiv* **2024**, arXiv:2411.16247.
28. Zhu, W.; Ma, W.; Su, Y.; Chen, Z.; Chen, X.; Ma, Y.; Bai, L.; Xiao, W.; Liu, T.; Zhu, H.; et al. Low-dose real-time X-ray imaging with nontoxic double perovskite scintillators. *Light. Sci. Appl.* **2020**, *9*, 112. [CrossRef]
29. Li, Y.; Shao, W.; Chen, L.; Wang, J.; Nie, J.; Zhang, H.; Zhang, S.; Gao, R.; Ouyang, X.; Ouyang, X.; et al. Lead-halide Cs4PbBr6 single crystals for high-sensitivity radiation detection. *NPG Asia Mater.* **2021**, *13*, 40. [CrossRef]
30. Lin, R.; Zhu, Y.; Chen, L.; Zheng, W.; Xu, M.; Ruan, J.; Li, R.; Li, T.; Lin, Z.; Cheng, L.; et al. Ultrafast (600 ps) α-ray scintillators. *PhotoniX* **2022**, *3*, 9. [CrossRef]
31. Zhang, J.; Dong, P.; Dang, K.; Zhang, Y.; Yan, Q.; Xiang, H.; Su, J.; Liu, Z.; Si, M.; Gao, J.; et al. Ultra-wide bandgap semiconductor Ga_2O_3 power diodes. *Nat. Commun.* **2022**, *13*, 3900. [CrossRef] [PubMed]
32. Galazka, Z. β- Ga_2O_3 for wide-bandgap electronics and optoelectronics. *Semicond. Sci. Technol.* **2018**, *33*, 113001. [CrossRef]
33. Usui, Y.; Kato, T.; Kawano, N.; Okada, G.; Kawaguchi, N.; Yanagida, T. Comparative study of scintillation properties of Ga_2O_3 single crystals and ceramics. *J. Lumin.* **2018**, *200*, 81–86. [CrossRef]
34. Usui, Y.; Oya, T.; Okada, G.; Kawaguchi, N.; Yanagida, T. Comparative study of scintillation and optical properties of Ga_2O_3 doped with ns2 ions. *Mater. Res. Bull.* **2017**, *90*, 266–272. [CrossRef]
35. Anand, A.; Zaffalon, M.L.; Cova, F.; Pinchetti, V.; Khan, A.H.; Carulli, F.; Brescia, R.; Meinardi, F.; Moreels, I.; Brovelli, S. Optical and Scintillation Properties of Record-Efficiency CdTe Nanoplatelets toward Radiation Detection Applications. *Nano Lett.* **2022**, *22*, 8900–8907. [CrossRef] [PubMed]
36. Huso, J.; McCluskey, M.D.; Yu, Y.; Islam, M.M.; Selim, F. Localized UV emitters on the surface of beta- Ga_2O_3. *Sci. Rep.* **2020**, *10*, 21022. [CrossRef] [PubMed]
37. Abram, R.A.; Rees, G.J.; Wilson, B.L.H. Heavily doped semiconductors and devices. *Adv. Phys.* **1978**, *27*, 799–892. [CrossRef]
38. Yang, X.; Tang, H.; Zhang, C.; Li, X.; Wang, W.; Huang, X.; Peng, X.; Zhang, C.; Xu, J.; Liu, B. Luminescence properties of β-Ga2O3: Bi single crystals growth by the optical floating zone method. *J. Lumin.* **2025**, *278*, 12100238. [CrossRef]
39. Li, X.; Chen, J.; Yang, D.; Chen, X.; Geng, D.; Jiang, L.; Wu, Y.; Meng, C.; Zeng, H. Mn^{2+} induced significant improvement and robust stability of radioluminescence in Cs3Cu2I5 for high-performance nuclear battery. *Nat. Commun.* **2021**, *12*, 3879. [CrossRef]
40. Kirm, M.; Nagirnyi, V.; Feldbach, E.; De Grazia, M.; Carré, B.; Merdji, H.; Guizard, S.; Geoffroy, G.; Gaudin, J.; Fedorov, N.; et al. Exciton-exciton interactions in $CdWO_4$ irradiated by intense femtosecond vacuum ultraviolet pulses. *Phys. Rev. B* **2009**, *79*, 233103. [CrossRef]
41. Aleksiejunas, R.; Podlipskas, Z.; Nargelas, S.; Kadys, A.; Kolenda, M.; Nomeika, K.; Mickevicius, J.; Tamulaitis, G. Direct Auger recombination and density-dependent hole diffusion in InN. *Sci. Rep.* **2018**, *8*, 4621. [CrossRef] [PubMed]
42. García Víllora, E.; Hatanaka, K.; Odaka, H.; Sugawara, T.; Miura, T.; Fukumura, H.; Fukuda, T. Luminescence of undoped β-Ga_2O_3 single crystals excited by picosecond X-ray and sub-picosecond UV pulses. *Solid State Commun.* **2003**, *127*, 385–388. [CrossRef]